Journal of Molecular Liquids 353 (2022) 118773

Contents lists available at ScienceDirect

Journal of Molecular Liquids

journal homepage: www.elsevier.com/locate/molliq

Fluorinated carbon and boron nitride fullerenes for drug Delivery: Computational study of structure and adsorption

Elizaveta B. Kalika [a,b], Konstantin P. Katin [a,c,*], Alexey I. Kochaev [a,d], Savas Kaya [e], Mustafa Elik [f], Mikhail M. Maslov [a,c]

[a] Laboratory of Computational Design of Nanostructures, Nanodevices, and Nanotechnologies, Research Institute for the Development of Scientific and Educational Potential of Youth, Aviatorov str. 14/55, Moscow 119620, Russia
[b] Moscow Institute of Physics and Technology (National Research University), 1 «A» Kerchenskaya st., Moscow 117303, Russia
[c] Department of Condensed Matter Physics, National Research Nuclear University "MEPhI", Kashirskoe Sh. 31, 115409 Moscow, Russia
[d] Research and Education Center "Silicon and Carbon Nanotechnologies", Ulyanovsk State University, 42 Leo Tolstoy Str., 432017 Ulyanovsk, Russia
[e] Department of Chemistry, Faculty of Science, Cumhuriyet University, Sivas 58140, Turkey
[f] Department of Mathematics and Science Education, Cumhuriyet University, Sivas 58000, Turkey

ARTICLE INFO

Article history:
Received 29 November 2021
Revised 31 January 2022
Accepted 15 February 2022
Available online 17 February 2022

Keywords:
Fluorination
Fluorinated fullerenes
$B_{12}N_{12}$
C_{60}
Drug delivery
Density functional theory

ABSTRACT

We applied a genetic algorithm combined with the B3LYP/6-311G** approach to determine the structures of low-energy isomers of partially fluorinated fullerenes, the number of which is combinatorically huge. We found that the effective interaction of fluorine atoms on the fullerene surface can not be described within the pair approximation with sufficient accuracy. For the smallest C_{20} fullerene, the most robust bonding with fluorine was observed in the $C_{20}F_2$ isomer, whereas further fluorination was less feasible. For C_{60} fullerene, the most thermodynamically stable isomers were $C_{60}F_2$ and $C_{60}F_m$ with *m* about 40. Effective attraction energy of adsorbed fluorine atom with OH, NH_2, and COOH functional groups on the C_{60} fullerene surface is about 1.24 eV. Vibration analysis of the stable $C_{60}F_m$ isomers clarified the frequencies shifts during the gradual fluorination. As to fluorinated derivatives of boron nitride cages, some of them possess extreme distortions under low fluorination. However, half- and fully-fluorinated BN fullerenes demonstrate moderate strain and strong van-der-Waals interaction with doxorubicin drug. Loading of doxorubicin on both carbon and boron nitride fullerenes with varying degrees of fluorination confirmed that fluorine concentration defines the energy of the fullerene-drug interaction. A half-fluorinated $B_{12}N_{12}F_{12}$ cage provides the most substantial adsorption, as the fluorine atoms on its surface are more moveable and can "adjust" to the DOX molecule.

1. Introduction

Targeted drug delivery (TDD) is increasingly used in modern medicine. The most efficient application of TDD is cancer treatment. It ensures the drug release in the tumor site without causing any damage to the extracellular environment and unwanted side effects. Many anticancer drugs have short half-lives and, therefore, may have concentration fluctuations, so a higher drug dose is needed. TDD can be used in such cases to reduce the drug dose and to avoid side effects caused by alternating drug concentration [1]. In recent years, TDD was used to treat many diseases beyond cancer, such as diabetes [2,3], cardiovascular [4], respiratory [5], and inflammatory [6] diseases.

Drug carrier is the fundamental part of TDD. It can be prepared from different types of materials, including organic and inorganic nanoparticles or polymer/inorganic nanocomposites with different morphologies [7]. However, their efficacy depends on many factors, such as their shape, size, chemical activity, and biological comparability.

The main stages of the TDD process are drug loading, delivery, and release. The interaction between drug and carrier plays a crucial role in all three stages. Drug loading implies strong chemical or van-der-Waals binding of the carrier with the drug or formation of host–guest endohedral complexes. Delivery and release stages are performed in different ways depending on the type of the drug carrier. The simplest way for drug release is breaking the drug-carrier bonds induced by pH, heat, or external fields. Another strategy implies carrier decomposition. For example, some polymeric nanocapsules, which transport drugs to the tumor cell site, can degrade due to an acidic environment [8]. On the other hand, lecithin-chitosan was confirmed as a promising carrier for topical

* Corresponding author.
E-mail address: KPKatin@yandex.ru (K.P. Katin).

https://doi.org/10.1016/j.molliq.2022.118773
0167-7322/

delivery of quercetin due to its high biodegradability [9]. More sophisticated strategies are also used in modern TDD systems. For example, in Ref. [8] micellar system containing drug molecules were created, antibodies and markers were attached to the hydrophilic tails of the micelles molecules, and then antibodies were bound to the antigen of the target tumor cell.

Carbon fullerenes possess many advantages as drug carriers [10,11]. In contrast to others nanoparticles, fullerenes' size and shape demonstrate well reproducibility [12]. In addition, they are bio-comparable non-toxic compounds. Similar to other sp^2-hybridized systems, each carbon atom of the fullerene can form a covalent bond with the drug, linker molecule of the functional group. On the other hand, the non-covalent interaction of fullerenes with the aromatic rings of the drug molecule is possible due to π-π coupling. Functionalization of fullerenes or embedding foreign atoms into the carbon cages allows tuning their adsorption properties, solubility, and bioactivity in a wide range [13,14]. In particular, carbon fullerenes-based TDD systems were found to be suitable for delivery of docetaxel [15], ibuprofen [16], amantadine [17], dopamine [18], and others drugs [19,20].

Boron nitride (BN) fullerenes keep most advantages of their carbon counterparts [21]. Moreover, the BN structures provide improved adsorption of organic functional groups such as NH_2. Furthermore, the presence of polar solvent (e.g., water) increases the binding of BN fullerenes with drugs [22 –25]. Therefore, BN fullerenes were recognized as a promising TDD basis for many drugs, such as sulfasalazine [26], ifosfamide [27], 5-fluorouracil [28], melphalan [29], and hydroxyurea [30].

In this study, we focus on fluorinated carbon and BN fullerenes. Although they were not earlier considered for TDD applications, they seem to be promising for several reasons. Firstly, fluorinated carbon nanoparticles are more preferable to TDD systems due to their intense near-infrared performance [31,32]. Secondly, fluorine provides the ability to detect a nanoparticle in the organism using nuclear magnetic resonance (NMR) [33] due to the clear signal and strong chemical shift of fluorine. Finally, fluorine possesses high electronegativity, which contributes to the non-covalent interaction of the fluorinated fullerene with the drugs. Recently, TDD systems for cancer treatment based on fluorinated graphene nanoflakes were successfully synthesized and tested [34]. Compared to the graphene nanoflakes, fullerenes exhibit a well-defined size, do not have highly reactive edges, and demonstrate improved adsorption due to surface curvature.

Although fluorinated graphene-based nanostructures are currently used for many applications [35,36], including drugs delivery [34,37,38], the structures of fluorinated fullerenes are still controversial. Highly fluorinated fullerenes can barely be synthesized even in extreme conditions [39]. In fact, researchers deal with a mix of partially fluorinated fullerenes, which have many isomers with different fluorine patterns on their surfaces and, therefore, various activities towards drugs. Here we aimed to clarify the structural features of fluorinated carbon and BN fullerenes and investigate fluorine's effect on their reactivity to drugs. We consider doxorubicin (DOX) as the most common example of a drug molecule that contains both typical reactive functional groups (=O, —OH, —NH_2) and conjugated aromatic rings, which are essential for interaction with fullerenes. Note that DOX has been used for cancer treatment for almost 50 years. Nevertheless, interest in it does not decrease, and the possibilities of its delivery with carbon nanostructures were actively investigated recently [40,41].

2. Computational details

B3LYP [42,43] exchange-corrected functional coupled with the 6-311G** electronic basic set [44] was used to conduct all the calculations. GPU-based TeraChem software was used for geometry optimization of all molecules [45] with the efficient geomeTRIC energy minimizer [46]. Dispersion corrections D3 by Grimme et al. [47] were introduced to take into account non-covalent interaction between drug and carrier. In TeraChem software, DFT algorithms are implemented in such a way that they can be executed on GPUs. Such architecture provides the usage of computational power of video cards in quantum calculations and speeds them up many times.

Finding the most stable isomers of partially fluorinated fullerenes is quite complicated because of the huge combinatorial number of possible isomers. On the other hand, the energy difference between two isomers due to the different relative positions of only two fluorine atoms is ~ 1 eV [48]. Therefore, only low-energy isomers can be synthesized. To recognize low-energy isomers, we created a script based on a genetic algorithm fitted to our particular goal instead of general-purpose evolutionary structure predictors like USPEX [49] or CALYPSO [50]. Our algorithm consisted of four stages. Firstly, the initial population of fullerenes functionalized by a given number of randomly distributed fluorine atoms is created. Then all the isomers in the population are optimized to select the best two isomers. During the next stage, six new isomers are created from this pair in a special way: half of the fluorines are bound in the same position as in the first "parent", and another half as in the second one. After that, a mutation is simulated: one randomly selected fluorine atom is moved to a new random position on the fullerene, while other fluorine atoms are fixed on the fullerene cage. The expanded population is then reduced to its original size by discarding "the worst" isomers with the highest energies. The process is iterated until the population does not stop improving within ten iterations. Population sizes were 10 and 20 isomers, whereas a typical number of iterations until convergence was about 100. Therefore, about 1000 isomers are probed. The algorithm was implemented with Python 3.7.3 and was integrated with TeraChem software and the geomeTRIC technique. Our approach provided using B3LYP/6-311G** level of theory for all calculations instead of applying simplified semiempirical methods for the genetic algorithm with further re-optimization with DFT of only the best structures. This is very important for our particular study because the semiempirical AM1 method, earlier used for genetic algorithm optimizing low-energy $C_{60}(CF_3)_n$ isomers [51], predicts qualitatively incorrect results for partially fluorinated fullerenes considered in our research. Time-consuming thermal corrections to energies were not considered because they were found to be negligible for comparing two isomers with different positions of functional groups in an interesting temperature range $300 \div 1000$ K [48]. Note that similar genetic algorithms are commonly used in couple with the DFT for global minima configurations search [52–54].

The selection of the best configurations for DOX loaded on the partially fluorinated fullerene was also a non-trivial task. There are many competitive non-covalent bonding mechanisms involving active functional groups (=O, —OH, —NH_2), π-π coupling, and direct electrostatic attraction. To get the best loading position, we applied "brute force" enumeration. Namely, we optimized dozens of different initial configurations obtained by alternating rotations of DOX molecule around the two perpendicular axes. One axis connected the centers of mass of the fluorinated fullerene and the drug, and the second axis passed through the center of mass of the drug perpendicular to the first axis. We used the same step of 20° for rotations in both directions. Note that the GPU-accelerated software allows us to perform the enumeration at the DFT level of theory. In contrast, previous studies used for this purpose simplified semiempirical or empirical approaches with further re-calculation of the best complexes only [55–57].

As a quantitative measure of the drug-fullerene interaction, we studied the adsorption energy E_{ads}, the distortion energy of fuller-

ene $E_{D(full)}$ and the drug $E_{D(drug)}$, and the interaction energy E_{int}. A well-known equation determined the adsorption energy

$$E_{ads} = E(\text{fullerene} - \text{drug complex}) - E(\text{fullerene}) - E(\text{drug}). \quad (1)$$

Negative value of the E_{ads} means that the complex is more energetically favorable than its parts considered separately. The distortion energy was defined as the difference between the single-point energy of the distorted fullerene/drug extracted from the complex and its energy calculated for the optimized geometry. The interaction energy can be estimated as the sum of three contributions:

$$E_{int} = E_{ads} + E_{D(full)} + E_{D(drug)}. \quad (2)$$

We also calculated the energies of the highest occupied (E_{HOMO}) and the lowest unoccupied (E_{LUMO}) molecular orbitals. Then we estimated quantum descriptors of reactivity (electronegativity χ, chemical hardness η, and electrophilicity index ω) from the energies of frontier molecular orbitals:

$$\chi \approx -(E_{HOMO} + E_{LUMO})/2; \quad (3)$$

$$\eta \approx (E_{LUMO} - E_{HOMO})/2; \quad (4)$$

$$\omega = \chi^2/(2\eta). \quad (5)$$

3. Results and discussion

3.1. Inapplicability of pair approximation for the interaction of fluorine atoms on the fullerene surface

Pair approximation is a very useful approach, which greatly reduces the computational resources due to neglecting many-body interactions. For our particular case of partially fluorinated carbon fullerenes, this approach implies that the energy E of the fullerene C_nF_m can be evaluated as

$$E \approx E(C_n) + m \cdot E(F) + m \cdot E(C - Fbond) + \sum_{i,j>i} E_{ij} \quad (6)$$

Here E_{ij} (i, j = 1 to m) is the effective pair interaction of two fluorines on the fullerene surface, introduced and calculated in Ref. [44]. For example, for the $C_{20}F_3$ system, where fluorines occupy neighboring A, B, and C sites at the same pentagon (one by one), the energy can be evaluated as

$$E(C_{20}F_3) \approx E(C_{20}) + 3E(F) + 3E_{C-F} + E_{AB} + E_{AC} + E_{BC} \quad (7)$$

According to Ref. [44], E_{C-F} = -4.293 eV, whereas $E_{AB} = E_{BC}$ and E_{AC} are equal to −0.320 and −0.167 eV, respectively. However, equation (7) underestimates the $E(C_{20}F_3)$ value by 0.65 eV. We tried applying (7) to other configurations C_nF_m (n = 20 and 60, m = 3 and 4) and got similar errors, which are too large to recognize the low-energy isomers properly. The non-pair character of fluorine - fluorine interaction can be explained by distortion of carbon cage due to fluorination. Based on our results, one can conclude that the pair approximation is inapplicable for the interaction of fluorine atoms on the fullerene surface. This is why we apply the genetic algorithm as described above.

3.2. Low energy isomers of partially fluorinated carbon fullerenes

The fullerenes family includes many cages, with C_{60} being the most common. Larger cages are known as higher fullerenes; C_{70} is the most widely known among them, whereas giant cages like C_{240} are much less standard. Cages smaller than C_{60} are known as lower fullerenes. The smallest possible fullerene is dodecahedral C_{20} [58]. It is very reactive due to high strain energy, but it keeps its identity for a long time in a gaseous phase [59], and its fluorinated and other derivatives are quite stable in solutions [60]. According to a previous extensive study of fullerenes functionalization [48], higher fullerenes demonstrate the same behavior as C_{60}, whereas lower fullerenes possess some features due to their high curvature. For this reason, we select two cages, C_{20} and C_{60}, for further consideration.

We applied the genetic algorithm to recognize low-energy isomers of partially fluorinated $C_{20}F_m$ cages with m = 1 to 20. The lowest energy isomers for some m are presented in Fig. 1. One can observe the formation of two "fluoric islands" on the opposite sides of the fullerene, which are growing with m and finally merge. The fullerene surface demonstrates concave curvature between the islands. Each new fluorine atom increases the concave curvature, making further fluorination less feasible. However, it was found that each new fluorine atom could be attached to the cage without any activation barrier.

Knowing the structures of the lowest energy isomers, we calculated the average energies E_{avg} of the C–F bonds as follows:

$$E_{avg}(m) = \frac{E(C_n) + m \cdot E(F) - E(C_nF_m)}{m} \quad (8)$$

where n = 20, m = 1 to 20. The results are presented in Fig. 2a. It was found that isomers with even m are more energy favorable than the ones with odd m. In general, the value of E_{avg} tends to decrease with m. This fact explains a low yield of highly fluorinated C_{20} observed experimentally even at high temperature and high fluorine concentrations [60]. As shown in Fig. 2a, $C_{20}F_2$ possesses the highest value of E_{avg} and is, therefore, the most energetically favorable product of C_{20} fluorination. The cage distortion energy E_D is also presented in Fig. 2a. The value of E_D is defined as the difference between the single-point energy of the carbon cage after removing fluorines without any structural relaxation and optimized fullerene energy. One can see a monotonic increase of E_D with m, associated with the cage swelling and formation of ripples common for sp^3-hybridized carbon surfaces.

Similar results for C_{60} fullerene are presented in Fig. 2b. The value of E_{avg} was calculated with the same formula (8), assuming n = 60. Since the application of the genetic algorithm to this larger fullerene is more time-consuming, we considered only some typical values of m from 1 to 60 (namely, m = 1, 2, 4, 12, 24, 36, 48, 49, 60). The $E_{avg}(m)$ curve for C_{60} is non-monotonic, in contrast with the case of C_{20}. The value of E_{avg} reaches its first maximum at m = 2, and second maximum with m in range 36 ÷ 48, whereas others isomers are less feasible. Such conclusion coincides with the experimental results of direct fullerene fluorination collected in review [39]: the maximal yield of fluorinated $C_{60}F_m$ corresponds to m about 40. The reason for the low output of highly fluorinated products is the same as for the case of C_{20}: fluorinated carbon atoms rise under the fullerene surface, and the rest carbon atoms between fluorinated regions get concave curvature and become less reactive to fluorine. The total strain energy of the C_{60} carbon skeleton achieves 50 eV, much more than that for the C_{20} frame. Nevertheless, we found that the attachment of the new fluorine atom is always a barrierless process independent of the current degree of fluorination. However, previous simulations proved that fully fluorinated $C_{60}F_{60}$ fullerene has higher energy than other tubular structures with the same composition [61].

3.3. Vibrational spectra of partially fluorinated C_{60} cages

Vibration frequency is a suitable indicator that reflects the dependence of C–C and C—F bonds rigidity on the degree of fluorination. Experimentally measured infrared active peaks corresponding to C–F covalent bonds belong to the 950 ÷ 1350 cm^{-1} range [62]. However, fluorines also change the rigidity of the nearest carbon–carbon bonds due to electron density redistribution. To highlight the effect of fluorination, we calculated vibrational spec-

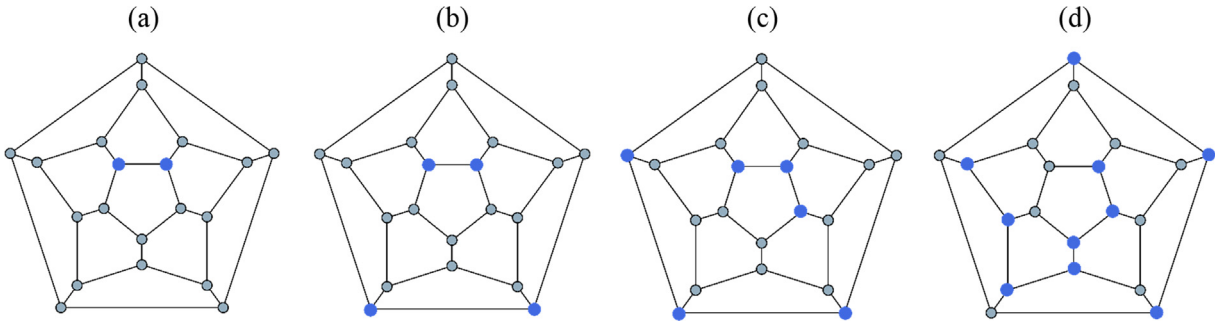

Fig. 1. Schlegel diagrams of the lowest energy isomers $C_{20}F_2$ (a), $C_{20}F_4$ (b), $C_{20}F_6$ (c), and $C_{20}F_{10}$ (d). Blue and grey points represent fluorinated and non-fluorinated sites of the fullerene, respectively. (For interpretation of the references to colour in this figure legend, the reader is referred to the web version of this article.)

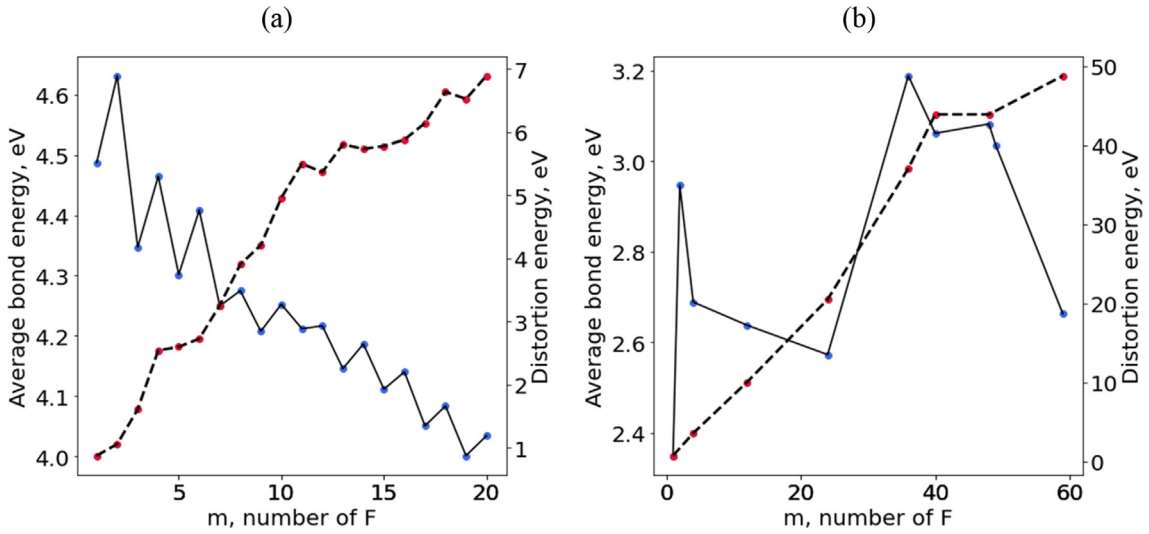

Fig. 2. Solid lines present average energies of C–F bonds for the lowest energy isomers of partially fluorinated fullerenes $C_{20}F_m$ (a) and $C_{60}F_m$ (b), calculated with the formula (3). Dashed lines are the cage distortion energies as functions of *m*.

tra of the most stable $C_{60}F$, $C_{60}F_2$, $C_{60}F_{36}$, and $C_{60}F_{48}$ isomers. Fig. 3 presents the difference in vibrational spectra of fluorinated systems with respect to pristine fullerene. Note that Fig. 4 illustrates not the absolute value of the vibrational frequencies density but the difference between the frequencies density of fluorinated and the pristine fullerene. This figure confirms that the fluorination leads to a shift in frequencies density from the range of 1400 ÷ 1600 cm^{-1} (in pristine fullerene) to the range of 1000 ÷ 1200 cm^{-1} (in fluorinated systems). In addition, fluorination contributes to the appearance of low-frequency oscillations associated with the "swinging" of fluorines relative to each other.

3.4. Interaction of fluorine with other active functional groups OH, NH_2, COOH on C_{60} surface

Although fluorine is the most electronegative element, there are other elements with high electronegativities, such as oxygen and nitrogen. These elements also can interact with drugs or linkers via hydrogen bonds or electrostatic interaction. The most common "active" groups are OH, NH_2 and COOH. Comparison of these groups with fluorine and their interaction on the fullerene surface can provide insight into the properties of cages co-functionalized with fluorine and other groups. As it was earlier established in Ref. [48], effective interaction energies of two functional groups F—F, F—OH, and OH—OH on the C_{60} surface in the most feasible *para* position are very close to each other (−1.18, −1.24 and

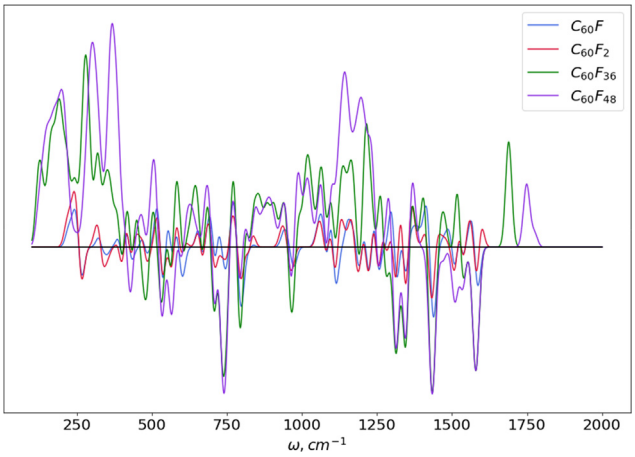

Fig. 3. Differences between vibrational densities of states for $C_{60}F$ (blue), $C_{60}F_2$ (red), $C_{60}F_{36}$ (green) or $C_{60}F_{48}$ (purple) and pristine C_{60} fullerene. The differences are calculated by subtraction of the vibrational state density of pristine fullerene from the vibrational states densities of fluorinated fullerenes. The uniform scaled factor of 0.98 was adopted from Ref. [63] and applied to all calculated frequencies. Gauss broadening with σ = 10 cm^{-1} was applied to each vibrational peak. Infrared activities of considered peaks were not taken into account in this figure (infrared spectra of fluorinated fullerenes are available in Supplementary materials Figs. S1-S4). (For interpretation of the references to colour in this figure legend, the reader is referred to the web version of this article.)

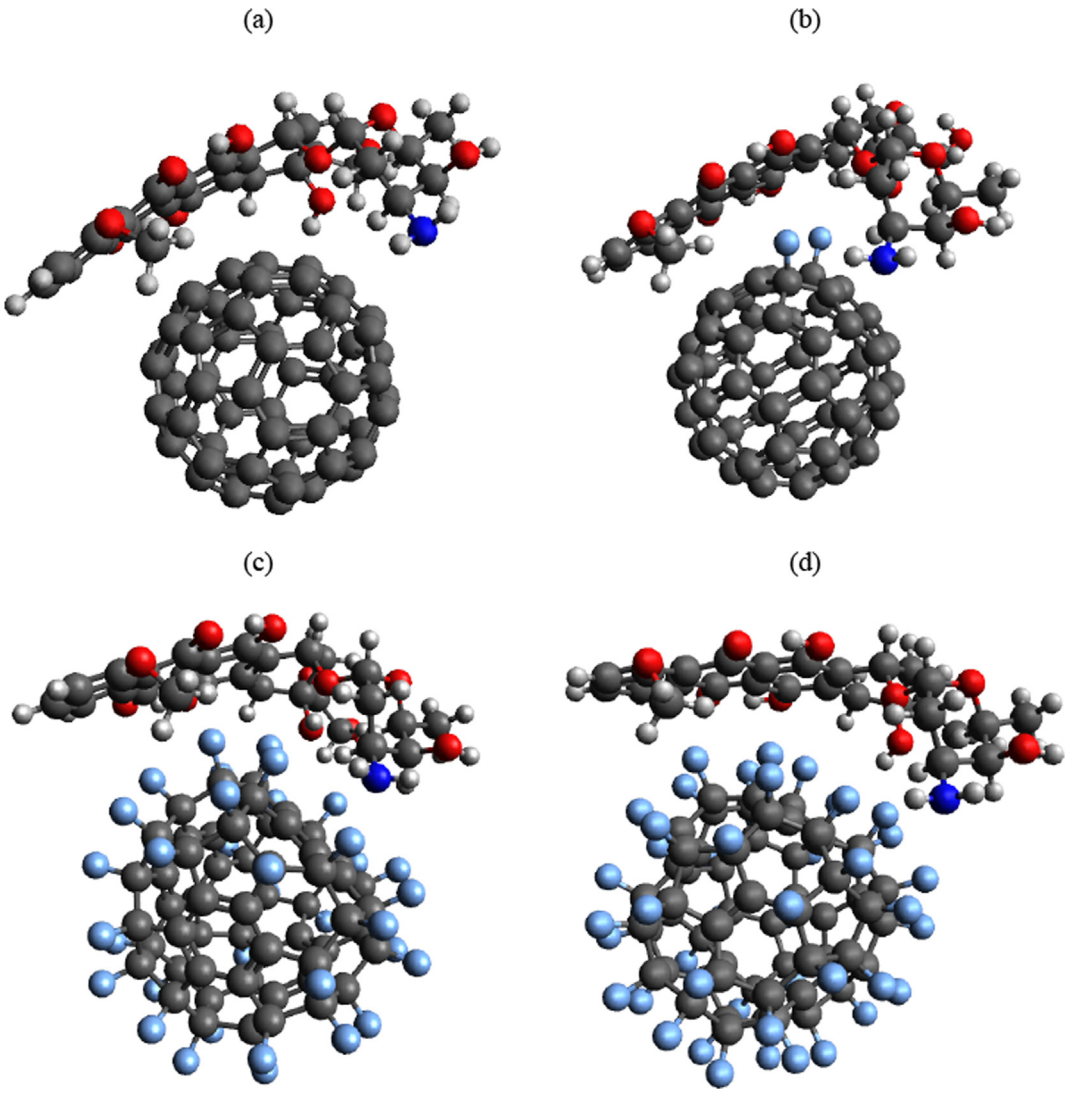

Fig. 4. Structures of DOX drug loaded on C_{60} (a), $C_{60}F_2$ (b) $C_{60}F_{36}$ (c) and $C_{60}F_{48}$ (d) fullerenes.

Table 1
Adsorption energies E_{ads} (eV), the distance between carbon and functional group l (Å), total Mulliken charges of the functional group q_M, and dipole moments d (Debye) for C_{60} fullerene functionalized with one "active" functional group. The data marked with an asterisk are adopted from the Ref. [44].

	E_{ads}	l	$q_M/\|e\|$	d
C_{60}–F	−2.21*	1.414*	−0.30*	0.72*
C_{60}–OH	−1.52*	1.433*	−0.18*	1.07*
C_{60}–NH_2	−1.20	1.480	−0.07	1.66
C_{60}–COOH	−1.20	1.546	0.04	1.47

−1.26 eV, respectively). However, NH_2 and COOH were not considered in Ref. [48]. Some calculated characteristics for the interaction of C_{60} with the "active" functional groups are presented in Table 1, whereas the effective energies of the interaction of these groups on the fullerene surface are collected in Table 2.

Numbers in Tables 1 and 2 confirmed that F demonstrated the strongest interaction with fullerene, whereas effective energies of pair interactions are approximately the same for all groups. The slightly weaker F-F interaction is explained by the impossibility of forming a hydrogen bond. Among other active groups, OH forms the strongest bond with the fullerene. Therefore, we conclude that OH is the most suitable group for co-functionalization.

3.5. Loading of DOX on the selected models of partially fluorinated fullerenes

To clarify the role of fluorine in the carrier-drug interaction, we loaded the DOX drug on C_{60}, $C_{60}F_2$, $C_{60}F_{36}$, and $C_{60}F_{48}$ fullerenes, which represent pristine, low-, middle- and highly-fluorinated carbon fullerenes, respectively. Note that earlier prepared and experimentally studied C_{60}-DOX complexes demonstrated high therapeutic efficiency [56,57]. According to previous studies, C_{60}-DOX or CNT-DOX binding is due to van-der-Waals attraction [64,65]. Therefore, fluorine atoms can reinforce their interactions significantly.

Table 2
Interaction energies E_i (eV) of two "active" functional groups adsorbed at the most feasible *para* position on the same hexagon of C_{60} fullerene. Definition of the E_i was adopted from Ref. [44]. The data marked with an asterisk were adopted from the same reference.

	F	OH	NH_2	COOH
F	−1.18*	−1.24*	−1.24	−1.25
OH	–	−1.26*	−1.24	−1.31
NH_2	–	–	−1.27	−1.27
COOH	–	–	–	−1.27

Table 3
Adsorption energies E_{ads}, distortion energies $E_{D(full)}$ and $E_{D(drug)}$, interaction energies E_{int}, frontier orbitals energies E_{HOMO} and E_{LUMO}, HOMO-LUMO gaps, electronegativity χ, chemical hardness η and electrophilicity index ω of the DOX drug loaded on the pristine and fluorinated C_{60} fullerene. All these values are in eV. The value of Δgap is the percentage change of the HOMO-LUMO gap due to DOX loading calculated as $((gap(C_{60}F_n - DOX) - gap(C_{60}F_n))/gap(C_{60}F_n)$ (n = 0, 2, 36, 48).

system	E_{ads}	$E_{D(full)}$	$E_{D(drug)}$	E_{int}	E_{HOMO}	E_{LUMO}	*gap*	χ	η	*w*	Δgap
C_{60} – DOX	0.57	0.01	0.62	1.19	−6.14	−3.62	2.52	4.88	1.26	9.44	−8%
$C_{60}F_2$ – DOX	1.09	0.02	0.15	1.25	−6.01	−3.06	2.95	4.53	1.48	6.96	+17%
$C_{60}F_{36}$ – DOX	1.17	0.02	0.41	1.59	−6.08	−4.44	1.64	5.26	0.82	16.85	−69%
$C_{60}F_{48}$ – DOX	0.59	0.01	0.63	1.23	−6.01	−5.20	0.81	5.61	0.40	38.90	−84%

Table 4
Bond energies E_b (eV) and lengths l (Å) for a single fluorine atom binding with BN cages $B_{12}N_{12}$ and $B_{16}N_{16}$. The values of E_b are calculated as $E_b = E$(BN cage) + E(F atom) − E (fluorinated cage). Partial Mulliken charges of fluorine atom q_F are also presented. The data marked with an asterisk are taken from Ref. [66].

	E_b	l_{B-N}	l_{B-F}	l_{N-F}	$q_F/\|e\|$	*d*
$B_{12}N_{12}$	–	1.438 ÷ 1.486	–	–	–	0.00
$B_{12}N_{12}F$ (F to B)	3.00/2.77*	1.427 ÷ 1.652	1.351	–	−0.21	2.59
$B_{12}N_{12}F$ (F to N)	0.67/0.59*	1.432 ÷ 1.491	–	2.022	−0.22	3.10
$B_{12}N_{12}F_{12}$	3.16	1.530 ÷ 1.583	1.350	–	−0.18	0.00
$B_{12}N_{12}F_{24}$	2.92	1.571 ÷ 1.627	1.330	1.414	−0.14	0.00
$B_{16}N_{16}$	–	1.455 ÷ 1.473	–	–	–	0.00
$B_{16}N_{16}F$ (F to B)	3.10	1.428 ÷ 1.618	1.359	–	−0.22	2.63
$B_{16}N_{16}F$ (F to N)	0.73	1.449 ÷ 1.479	–	2.020	−0.24	3.29
$B_{16}N_{16}F_{32}$	2.66	1.604 ÷ 1.636	1.328 ÷ 1.337	1.418 ÷ 1.427	−0.14	0.00

The adsorption energies and other energy characteristics of the "fluorinated fullerenes + DOX" complexes are presented in Table 3, whereas their structures are shown in Fig. 4. It can be seen that fluorine plays an important role in fullerene-drug binding. Fig. 4 confirms that the $C_{60}F_2$ and $C_{60}F_{36}$ cages interact with the drug molecule via both fluorinated and non-fluorinated parts of their surfaces. Such a type of loading provides smaller deformation of the drug and leads to higher adsorption energy compared to the pristine or highly fluorinated fullerenes C_{60} and $C_{60}F_{48}$ (see Table 4). Note that both pristine and fluorinated fullerenes are sufficiently rigid, and their distortion energies are negligible.

One can see from the last column of the table, that the gap of low-fluorinated fullerenes changes slightly due to DOX loading. In contrast, highly fluorinated fullerenes exhibit a strong gap reduction when loaded with DOX. This is because the HOMO orbitals of pristine fluorinated fullerenes have low energies, and therefore their HOMO-LUMO gaps are much higher.

3.6. Fluorinated BN cages

The structure and properties of partially fluorinated $B_{12}N_{12}$ cages have been investigated previously at the B3LYP/6-31G* level of theory [66]. According to the conclusions of Ref. [66], the average interaction energy of the BN cage with the fluorine atom monotonically decreases with the increase in the degree of fluorination. $B_{12}N_{12}F_2$ was recognized as the most stable fluorinated cage. However, the formation of full fluorinated cage $B_{12}N_{12}F_{24}$ was found to be feasible at temperatures below 1200 K.

To validate and extend the results of the previous study [66], we firstly investigated the interaction of a single fluorine atom with $B_{12}N_{12}$ and $B_{16}N_{16}$ cages. Our results confirm that fluorine atom can form a bond with both B and N atoms. Characteristics of these bonds are collected in Table 4. Adsorption energies are satisfactory comparable with the same results from Ref. [66] calculated with a smaller electronic basis. It was not surprising that the F–B interaction was much stronger than F–N. We found that adding the second fluorine atom to the same square cycle on the BN cage surface results in the highest energy gain, in accordance with the previous study [66]. However, we concluded that the second fluorine atom leads to a significant weakening of the BN cage. Fluorine-induced structural changes in BN cages are shown in Fig. 5. Fluorination of two boron atoms (Fig. 1b and e) leads to an extremely short distance between two nitrogen atoms of ∼ 1.66 Å, which is close to the single N-N bond length of 1.57 Å measured in nitramide. Fluorination of the neighboring boron and nitrogen atoms (Fig. 1c and f) leads to the elongation of corresponding B-N bonds to 1.85 Å, much more than the maximal value of a single B-N bond of 1.70 Å [67]. Such changes in bond lengths indicate the possibility of structural rearrangements in the BN cage. Therefore, we believe that the low-fluorinated BN cages demonstrate lower kinetic stability. Further NBO analysis combined with the molecular dynamics simulations can clarify the degree of stability of low-fluorinated BN cages. However, these investigations are beyond the aims of the presented paper.

It is remarkable that for half and fully fluorinated $B_{12}N_{12}F_{12}$, $B_{12}N_{12}F_{24}$, and $B_{16}N_{16}F_{32}$ cages, the lengths of all B–N bonds return to reasonable values (see Table 4). Therefore, half and fully fluorinated cages are presumed to be less strained and more kinetically stable. Note that we could not find a stable geometry of the $B_{16}N_{16}F_{16}$ cluster, which has all boron atoms fluorinated. We tried

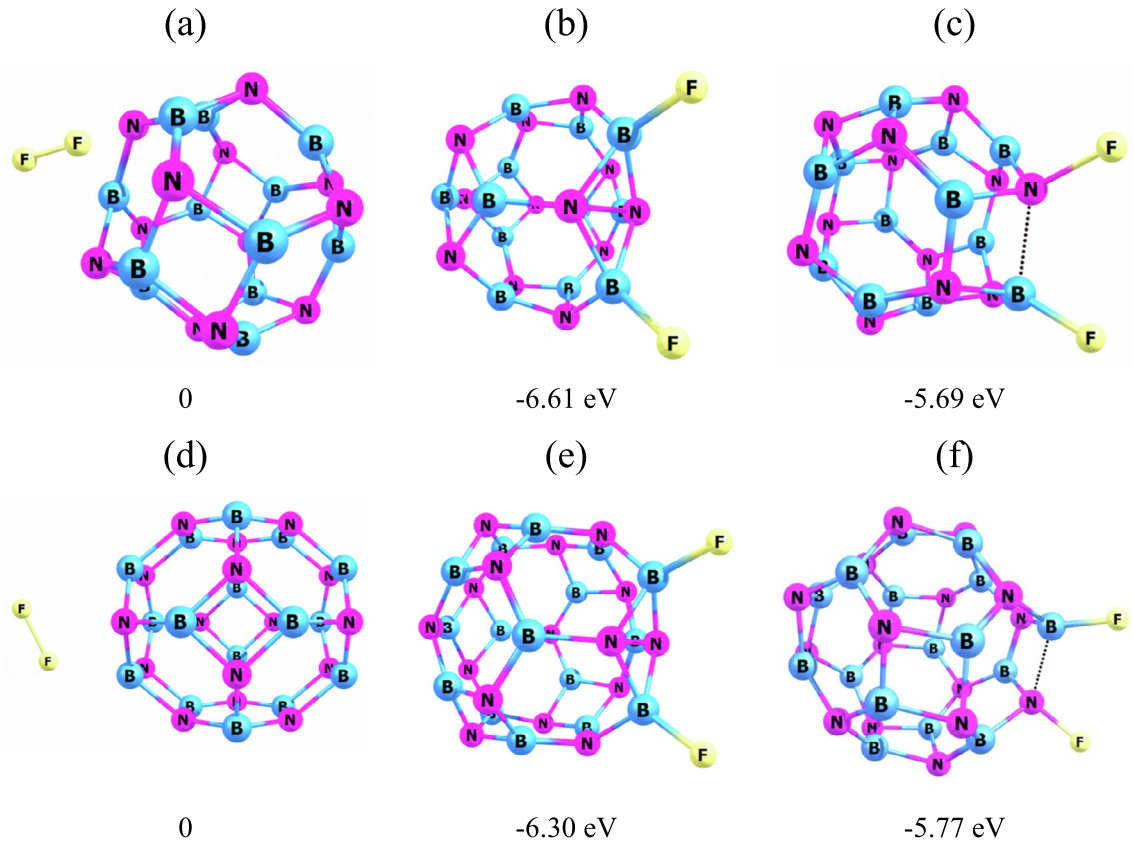

Fig. 5. Optimized atomic structures of different $B_{12}N_{12}F_2$ (a-c) and $B_{16}N_{16}F_2$ (d-f) configurations and their relative energies. The energies of configurations (a) and (d) are selected as zero points.

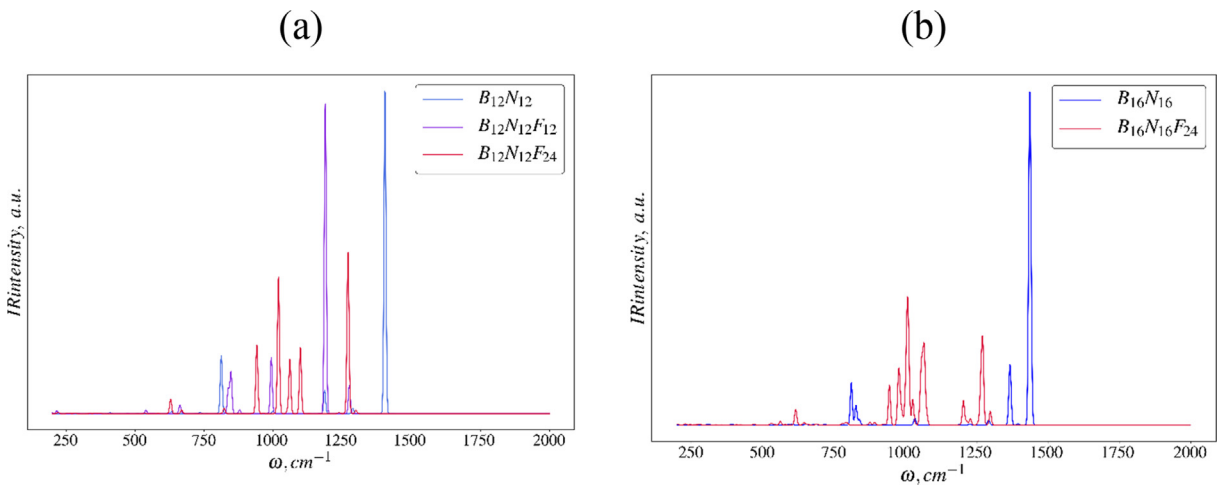

Fig. 6. Calculated infrared spectra of $B_{12}N_{12}$, $B_{12}N_{12}F_{12}$, $B_{12}N_{12}F_{24}$ (a) and $B_{16}N_{16}$, $B_{16}N_{16}F_{32}$ cages. Gauss broadening with σ = 10 cm^{-1} was applied to each vibrational peak. The uniform scaled factor of 0.99 was applied to all frequencies to achieve matching with the results previously obtained for $B_{12}N_{12}$ in Ref. [24].

numerous initial geometries, but the cluster structure always broke down during relaxation. We have concluded that this cluster is unstable or has very low stability.

For further DOX drug loading, we focused on $B_{12}N_{12}F_{12}$, $B_{12}N_{12}F_{24}$, and $B_{16}N_{16}F_{32}$ cages only. They were chosen not only because of lower strain: unlike carbon fullerenes, BN cages typically form covalent bonds with oxygen or nitrogen atoms of the drug molecules [29,68,69]. This is mainly due to the high chemical activity of boron. Covalent binding has both some advantages and disadvantages compared to the van-der-Waals binding. However, here we focus on non-covalent mechanisms of binding, as is the case of carbon fullerenes. Full fluorination of boron atoms eliminates the possibility of covalent binding. For this reason, we chose $B_{12}N_{12}F_{12}$, $B_{12}N_{12}F_{24}$, and $B_{16}N_{16}F_{32}$ clusters instead of more thermodynamically favorable low-fluorinated fullerenes like $B_{12}N_{12}F_2$. The characteristics of the selected models of BN cages are listed in Table 4. Fluorinated $B_{12}N_{12}$ and $B_{16}N_{16}$ have similar properties, as the corresponding bond lengths and dipole moments differ slightly. It is not surprising that the negative charge transfer to fluorine atoms decreases with an increase in the number of fluorines (see Table 4).

Fig. 6 presents calculated IR spectra of fluorinated BN cages, which have not been published previously. In accordance with the previous studies, the characteristic peak of the pristine

Table 5
Adsorption energies E_{ads}, distortion energies $E_{D(full)}$ and $E_{D(drug)}$, interaction energies E_{int}, frontier orbitals energies E_{HOMO} and E_{LUMO}, HOMO-LUMO gaps, electronegativity χ, chemical hardness η and electrophilicity index ω of the DOX drug loaded on the half- and fully fluorinated $B_{12}N_{12}$ and $B_{16}N_{16}$ cages. Pristine cages were not considered because they can form covalent bonds with the drug. All values are in eV.

system	E_{ads}	$E_{D(full)}$	$E_{D(drug)}$	E_{int}	E_{HOMO}	E_{LUMO}	*gap*	χ	η	*w*
$B_{12}N_{12}F_{12}$ – DOX	1.48	0.95	1.17	3.60	−6.49	−5.98	0.51	6.23	0.26	75.54
$B_{12}N_{12}F_{24}$ – DOX	0.69	0.03	0.55	1.28	−6.13	−5.35	0.78	5.74	0.39	42.45
$B_{16}N_{16}F_{32}$ – DOX	0.53	0.00	0.58	1.11	−6.25	−5.75	0.50	6.00	0.25	72.63

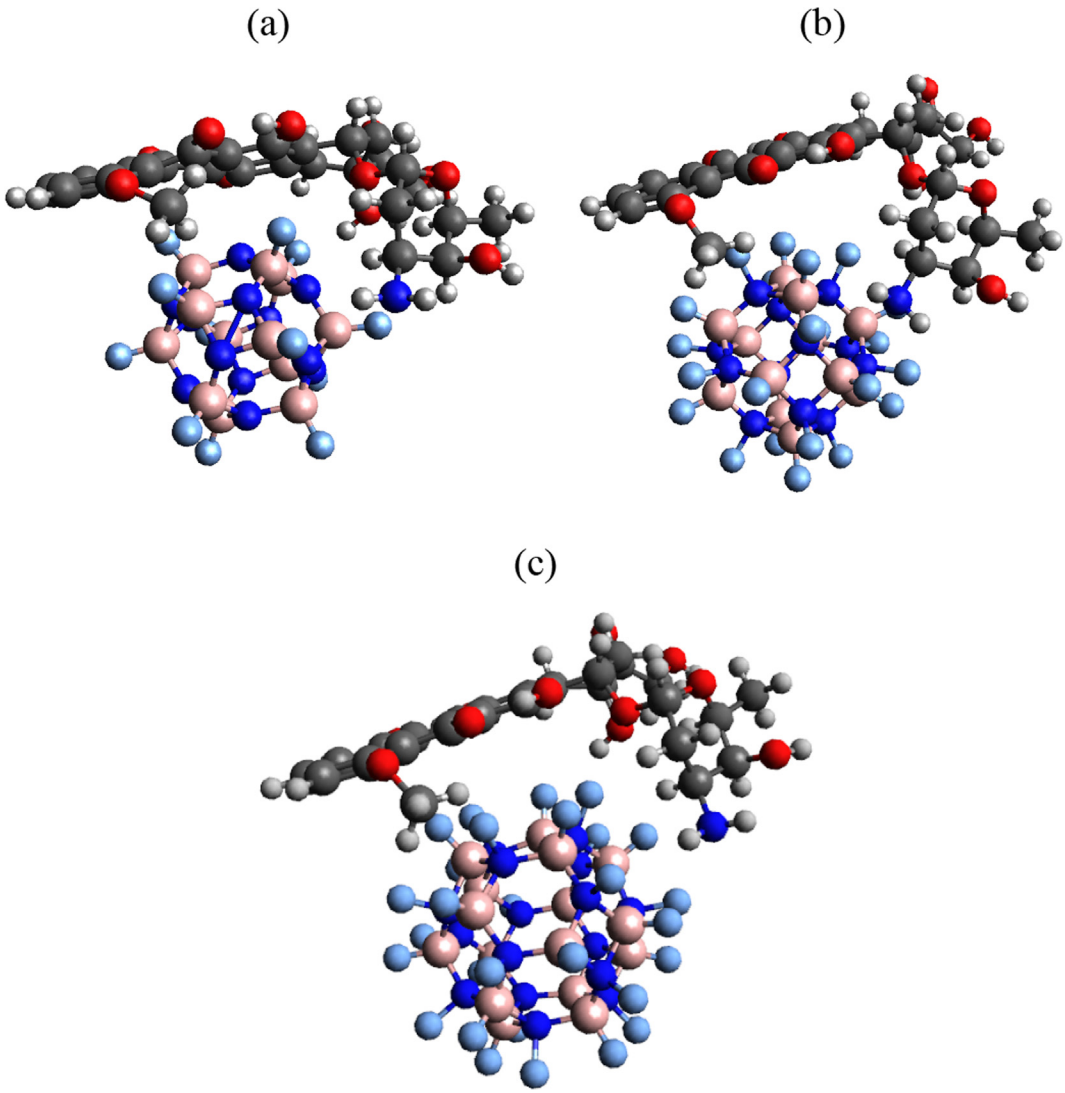

Fig. 7. Structures of the DOX drug loaded on $B_{12}N_{12}F_{12}$ (a), $B_{12}N_{12}F_{24}$ (b) and $B_{16}N_{16}F_{32}$ (c) cages.

$B_{12}N_{12}$ cage at 1403 cm^{-1} represents the stretching vibrations of the B—N bond, while peaks at 1180 cm^{-1} and 801 cm^{-1} represent the bending of B—N [26]. Fluorination leads to significant shifting of the peaks (see Fig. 6) and, therefore, can be easily detected by spectroscopic techniques.

3.7. Loading of DOX on the selected models of fluorinated BN cages

As explained above, in our research, we studied only fluorinated cages $B_{12}N_{12}F_{12}$, $B_{12}N_{12}F_{24,}$ and $B_{16}N_{16}F_{32}$, in which all boron atoms are passivated with fluorine and cannot form covalent bonds with the drug molecule. The energy characteristics of the obtained complexes are presented in Table 5, whereas their structure is shown in Fig. 7. The half-fluorinated $B_{12}N_{12}F_{12}$ cluster demonstrates the highest adsorption energy. Unlike carbon and fully fluorinated BN fullerenes, the fluorine atoms on its surface are placed far enough from each other. Therefore, they can rotate, adjust to the drug molecule and provide stronger adsorption. For this reason, $B_{12}N_{12}F_{12}$ possesses adsorption energy of about 1.5 eV, significantly higher than the other carbon and boron-nitride fullerenes considered in our research.

4. Conclusion

Carbon nanostructures and their BN counterparts retain their leading positions in drug delivery and in other applications due to the possibility of their modification. The addition of functional groups, preserving the structure of the carbon cage, makes it possible to obtain a wide variety of nanostructures with different properties. These properties are determined not only by the nature

of functional groups but also by their mutual arrangement. A direct theoretical study of all possible patterns formed by functional groups is usually impossible. Therefore, it is important to understand the features of the effective interaction of functional groups on the surface of the nanostructure that determines the resulting pattern. In this paper, we described the structural features of fluorinated carbon and BN fullerenes and examined their interaction with the DOX drug molecule. This particular case is important because we believe that the described approach can be applied to other functional groups that provide the necessary properties of carbon and BN nanostructures.

The main conclusions of this study are as follows. (i) For small fullerenes C_{20}, $B_{12}N_{12,}$ and $B_{16}N_{16}$, the most thermodynamically stable fluorinated derivatives have two fluorine atoms only. For fullerene C_{60}, $C_{60}F_m$ isomers with *m* about 40 are also feasible. (ii) Low-fluorinated boron-nitride fullerenes are very strained and probably low kinetically stable. (iii) Fluorine enhances vander-Waals attraction between fullerene and the drug significantly. Half-fluorinated fullerenes provide stronger adsorption. Both fluorinated and non-fluorinated parts of the carbon fullerene surface are important for drug loading. (iv) The half-fluorinated $B_{12}N_{12}F_{12}$ cluster demonstrates the highest adsorption energy because its fluorine atoms have the ability to deviate from their pristine positions, "adjusting" to the drug molecule.

CRediT authorship contribution statement

Elizaveta B. Kalika: Methodology, Software, Validation, Formal analysis, Data curation, Writing – review & editing. **Konstantin P. Katin:** Conceptualization, Methodology, Software, Validation, Formal analysis, Investigation, Data curation, Writing – original draft, Project administration, Funding acquisition. **Alexey I. Kochaev:** Software, Validation, Formal analysis, Data curation, Writing – review & editing. **Savas Kaya:** Software, Validation, Formal analysis, Data curation. **Mustafa Elik:** Software, Data curation. **Mikhail M. Maslov:** Conceptualization, Methodology, Software, Validation, Formal analysis, Investigation, Data curation, Writing – original draft.

Declaration of Competing Interest

The authors declare that they have no known competing financial interests or personal relationships that could have appeared to influence the work reported in this paper.

Acknowledgments

The presented study was performed with the financial support of the Russian Science Foundation (Grant No. 20-73-00245). Konstantin P. Katin is extremely grateful to DSEPY-RI for the provided computing resources and software as well as comprehensive support of the presented study.

Appendix A. Supplementary material

Supplementary data to this article can be found online at https://doi.org/10.1016/j.molliq.2022.118773.

References

[1] K.S. Yadav, D.K. Mishra, A. Deshpande, A.M. Pethe, Levels of Drug Targeting, Basic Fundamentals of, Drug Delivery (2019) 269–305, https://doi.org/10.1016/b978-0-12-817909-3.00007-8.
[2] L. Zhao, L. Wang, Y. Zhang, S. Xiao, F. Bi, J. Zhao, G. Gai, J. Ding, Glucose Oxidase-Based Glucose-Sensitive Drug Delivery for Diabetes Treatment, Polymers. 9 (2017) 255, https://doi.org/10.3390/polym9070255.
[3] L. Zhao, Q. Huang, Y. Liu, Q. Wang, L. Wang, S. Xiao, F. Bi, J. Ding, Boronic Acid as Glucose-Sensitive Agent Regulates Drug Delivery for Diabetes Treatment, Materials 10 (2017) 170, https://doi.org/10.3390/ma10020170.
[4] Y. Deng, X. Zhang, H. Shen, Q. He, Z. Wu, W. Liao, M. Yuan, Application of the Nano-Drug Delivery System in Treatment of Cardiovascular Diseases, Front. Bioeng. Biotechnol. 7 (2020), https://doi.org/10.3389/fbioe.2019.00489.
[5] M. Mehta, D. Deeksha, G. Tewari, R. Gupta, H. Awasthi, P. Singh, D.K. Pandey, R. Chellappan, T. Wadhwa, P.M. Collet, S.R. Hansbro, L. Kumar, P. Thangavelu, K. Negi, S. Dua, Satija, Oligonucleotide therapy: An emerging focus area for drug delivery in chronic inflammatory respiratory diseases, Chemico-Biol. Interactions 308 (2019) 206–215, https://doi.org/10.1016/j.cbi.2019.05.028.
[6] Y. Dou, C. Li, L. Li, J. Guo, J. Zhang, Bioresponsive drug delivery systems for the treatment of inflammatory diseases, J. Control. Release 327 (2020) 641–666, https://doi.org/10.1016/j.jconrel.2020.09.008.
[7] N. Salahuddin, A. Galal, Improving chemotherapy drug delivery by nanoprecision tools, Nanostructures for, Cancer Ther. (2017) 87–128, https://doi.org/10.1016/b978-0-323-46144-3.00004-0.
[8] N. Singh, A. Joshi, A.P. Toor, G. Verma, Drug delivery: advancements and challenges, Nanostructures for Drug Delivery (2017) 865–886, https://doi.org/10.1016/b978-0-323-46143-6.00027-0.
[9] Q. Tan, W. Liu, C. Guo, G. Zhai, Preparation and evaluation of quercetin-loaded lecithin-chitosan nanoparticles for topical delivery, IJN (2011) 1621, https://doi.org/10.2147/ijn.s22411.
[10] A. Montellano, T. Da Ros, A. Bianco, M. Prato, Fullerene C60 as a multifunctional system for drug and gene delivery, Nanoscale 3 (2011) 4035, https://doi.org/10.1039/c1nr10783f.
[11] M. Kumar, K. Raza, C_{60}-fullerenes as Drug Delivery Carriers for Anticancer Agents: Promises and Hurdles, PNT 5 (2018), https://doi.org/10.2174/2211738505666170301142232.
[12] M. Kurban, İ. Muz, Theoretical Investigation of the Adsorption Behaviors of Fluorouracil as an Anticancer Drug on Pristine and B-, Al-, Ga-Doped C36 Nanotube, J. Mol. Liq. 309 (2020), https://doi.org/10.1016/j.molliq.2020.113209 113209.
[13] İ. Muz, M. Kurban, A first-principles evaluation on the interaction of 1,3,4-oxadiazole with pristine and B-, Al-, Ga-doped C_{60} fullerenes, J. Mol. Liq. 335 (2021), https://doi.org/10.1016/j.molliq.2021.116181 116181.
[14] İ. Muz, F. Göktaş, M. Kurban, A density functional theory study on favipiravir drug interaction with BN-doped C60 heterofullerene, Physica E 135 (2022) 114950, https://doi.org/10.1016/j.physe.2021.114950.
[15] J. Shi, H. Zhang, L. Wang, L. Li, H. Wang, Z. Wang, Z. Li, C. Chen, L. Hou, C. Zhang, Z. Zhang, PEI-derivatized fullerene drug delivery using folate as a homing device targeting to tumor, Biomaterials 34 (1) (2013) 251–261, https://doi.org/10.1016/j.biomaterials.2012.09.039.
[16] E. Alipour, F. Alimohammady, A. Yumashev, A. Maseleno, Fullerene C60 containing porphyrin-like metal center as drug delivery system for ibuprofen drug, J. Mol. Model. 26 (2019), https://doi.org/10.1007/s00894-019-4267-1.
[17] C. Parlak, Ö. Alver, A density functional theory investigation on amantadine drug interaction with pristine and B, Al, Si, Ga, Ge doped C60 fullerenes, Chem. Phys. Lett. 678 (2017) 85–90, https://doi.org/10.1016/j.cplett.2017.04.025.
[18] A.S. Rad, M.H. Shahavi, M.R. Esfahani, N. Darvishinia, S. Ahmadizadeh, Are nickel- and titanium- doped fullerenes suitable adsorbents for dopamine in an aqueous solution? Detailed DFT and AIM studies, J. Mol. Liq. 322 (2021), https://doi.org/10.1016/j.molliq.2020.114942 114942.
[19] M. Nouraliei, M. Karimkhani, S. Mansouri, Z. Bagheri, Geometry-controlled carbon nanostructures as effective drug delivery carriers for MAO enzyme inhibitors: A DFT study, J. Mol. Liq. 340 (2021) 116857, https://doi.org/10.1016/j.molliq.2021.116857.
[20] W. Li, T. Zhao, Hydroxyurea anticancer drug adsorption on the pristine and doped C70 fullerene as potential carriers for drug delivery, J. Mol. Liq. 340 (2021), https://doi.org/10.1016/j.molliq.2021.117226 117226.
[21] İ. Muz, F. Göktaş, M. Kurban, Size Dependence in the Electronic and Optical Properties of a BN Analogue of Two-Dimensional Graphdiyne: A Theoretical Study, Chem. Phys. 539 (2020), https://doi.org/10.1016/j.chemphys.2020.110929 110929.
[22] A.S. Ghasemi, M.R. Taghartapeh, A. Soltani, P.J. Mahon, Adsorption behavior of metformin drug on boron nitride fullerenes: Thermodynamics and DFT studies, J. Mol. Liq. 275 (2019) 955–967, https://doi.org/10.1016/j.molliq.2018.11.124.
[23] N. Abdolahi, M. Aghaei, A. Soltani, Z. Azmoodeh, H. Balakheyli, F. Heidari, Adsorption of Celecoxib on B12N12 fullerene: Spectroscopic and DFT/TD-DFT study, Spectrochim. Acta Part A Mol. Biomol. Spectrosc. 204 (2018) 348–353, https://doi.org/10.1016/j.saa.2018.06.077.
[24] A. Soltani, M. Baei, A DFT Study on Structure and Electronic Properties of BN Nanostructures Adsorbed with Dopamine, Computation 7 (2019) 61, https://doi.org/10.3390/computation7040061.
[25] Y. Cao, A. Khan, H. Mirzaei, S. Reza Khandoozi, M. Javan, A. Ng Kay, A. Lup, E. Tazikeh Lemeski, M. Pishnamazi, A. Soltani, A.B. Albadarin, Investigations of adsorption behavior and anticancer activity of curcumin on pure and platinum-functionalized B12N12 nanocages, J. Mol. Liq. 334 (2021), https://doi.org/10.1016/j.molliq.2021.116516.
[26] N. Abdolahi, P. Singla, A. Soltani, M. Javan, M. Aghaei, F. Heidari, S. Sedighi, Gold decorated $B_{12}N_{12}$ nanocluster as an effective sulfasalazine drug carrier: A theoretical investigation, Physica E 124 (2020), https://doi.org/10.1016/j.physe.2020.114296 114296.
[27] A. Soltani, E. Tazikeh-Lemeski, M.B. Javan, A comparative theoretical study on the interaction of pure and carbon atom substituted boron nitride fullerenes

with ifosfamide drug, J. Mol. Liq. 297 (2020), https://doi.org/10.1016/j.molliq.2019.111894 111894.
[28] M.B. Javan, A. Soltani, Z. Azmoodeh, N. Abdolahi, N. Gholami, A DFT study on the interaction between 5-fluorouracil and $B_{12}N_{12}$ nanocluster, RSC Adv. 6 (106) (2016) 104513–104521.
[29] C.A. Celaya, L.F. Hernández-Ayala, F. Buendía Zamudio, J.A. Vargas, M. Reina, Adsorption of melphalan anticancer drug on C_{24}, $B_{12}N_{12}$, $B_{12}C_6N_6$, $B_6C_{12}N_{12}$ and $B_6C_6N_{12}$ nanocages: A comparative DFT study, J. Mol. Liq. 329 (2021) 115528, https://doi.org/10.1016/j.molliq.2021.115528.
[30] Z. Liao, G. Song, Z. Yang, H. Ren, Adsorption and desorption behaviors of hydroxyurea drug on delivery systems of $B_{12}N_{12}$ fullerene and its Al-, Si- and P-dopings from theoretical perspective, Mol. Phys. (2021), https://doi.org/10.1080/00268976.2021.1921296 e1921296.
[31] L.u. Sun, P. Gong, X. Liu, M. Pang, M. Tian, J. Chen, J. Du, Z. Liu, Fluorinated carbon fiber as a novel nanocarrier for cancer chemo-photothermal therapy, J. Mater. Chem. B. 5 (30) (2017) 6128–6137.
[32] L. Zhang, M. Wang, F. Kong, S. Li, G. Dai, P. Gong, Z. Liu, J. You, Synthesis of novel nanosized fluorinated carbon fiber with high NIR absorption and its application in cancer chemo-photothermal therapy, Mater. Lett. 244 (2019) 39–42, https://doi.org/10.1016/j.matlet.2019.02.056.
[33] R. Romero-Aburto, T.N. Narayanan, Y. Nagaoka, T. Hasumura, T.M. Mitcham, T. Fukuda, P.J. Cox, R.R. Bouchard, T. Maekawa, D.S. Kumar, S.V. Torti, S.A. Mani, P. M. Ajayan, Fluorinated Graphene Oxide; a New Multimodal Material for Biological Applications, Adv. Mater. 25 (39) (2013) 5632–5637, https://doi.org/10.1002/adma201301804.
[34] A. Khosravanian, A. Moslehipour, H. Ashrafian, A review on Bioimaging, Biosensing, and Drug Delivery Systems Based on Graphene Quantum Dots, Prog. Chem. Biochem. Res. (2020), https://doi.org/10.22034/pcbr.2020.237134.1102.
[35] N.A. Nebogatikova, I.V. Antonova, A.I. Ivanov, V.A. Demin, D.G. Kvashnin, A. Olejniczak, A.K. Gutakovskii, K.A. Kornieieva, P.L.J. Renault, V.A. Skuratov, L.A. Chernozatonskii, Fluorinated graphene nanoparticles with 1–3 nm electrically active graphene quantum dots, Nanotechnology 31 (2020), https://doi.org/10.1088/1361-6528/ab83b8 295602.
[36] I.V. Antonova, I.I. Kurkina, A.K. Gutakovskii, I.A. Kotin, A.I. Ivanov, N.A. Nebogatikova, R.A. Soots, S.A. Smagulova, Fluorinated graphene suspension for flexible and printed electronics: Flakes, 2D films, and heterostructures, Mater. Des. 164 (2019), https://doi.org/10.1016/j.matdes.2018.11.061 107526.
[37] P. Gong, Q. Zhao, D. Dai, S. Zhang, Z. Tian, L.u. Sun, J. Ren, Z. Liu, Functionalized Ultrasmall Fluorinated Graphene with High NIR Absorbance for Controlled Delivery of Mixed Anticancer Drugs, Chem. Eur. J. 23 (69) (2017) 17531–17541, https://doi.org/10.1002/chem.201702917.
[38] P. Gong, S. Ji, J. Wang, D. Dai, F. Wang, M. Tian, L. Zhang, F. Guo, Z. Liu, Fluorescence-switchable ultrasmall fluorinated graphene oxide with high near-infrared absorption for controlled and targeted drug delivery, Chem. Eng. J. 348 (2018) 438–446, https://doi.org/10.1016/j.cej.2018.04.193.
[39] O.V. Boltalina, N.A. Galeva, Direct fluorination of fullerenes, Russ. Chem. Rev. 69 (7) (2000) 609–621.
[40] S. Karimzadeh, B. Safaei, T. Jen, Prediction Effect of Ethanol Molecules on Doxorubicin Drug Delivery Using Single-Walled Carbon Nanotube Carrier through POPC Cell Membrane, J. Mol. Liq. 330 (2020), https://doi.org/10.1016/j.molliq.2021.115698 115698.
[41] S. Karimzadeh, B. Safaei, T. Jen, Investigate the Importance of Mechanical Properties of SWCNT on Doxorubicin Anti-Cancer Drug Adsorption for Medical Application: A Molecular Dynamic Study, J. Mol. Graph. Model. 101 (2020), https://doi.org/10.1016/j.jmgm.2020.107745 107745.
[42] A.D. Becke, Density-functional thermochemistry. III. The role of exact exchange, J. Chem. Phys. 98 (7) (1993) 5648–5652, https://doi.org/10.1063/1.464913.
[43] C. Lee, W. Yang, R.G. Parr, Development of the Colle-Salvetti correlation-energy formula into a functional of the electron density, Phys. Rev. B. 37 (2) (1988) 785–789.
[44] M. Tanaka, M. Katouda, S. Nagase, Optimization of RI-MP2 Auxiliary Basis Functions for 6–31G** and 6–311G** Basis Sets for First-, Second-, and Third-Row Elements, J. Comput. Chem. 34 (29) (2013) 2568–2575, https://doi.org/10.1002/jcc.23430.
[45] S. Seritan, C. Bannwarth, B.S. Fales, E.G. Hohenstein, S.I.L. Kokkila-Schumacher, N. Luehr, J.W. Snyder Jr., C. Song, A.V. Titov, I.S. Ufimtsev, T.J. Martínez, TeraChem: Accelerating electronic structure and ab initio molecular dynamics with graphical processing units, J. Chem. Phys. 152 (2020), https://doi.org/10.1063/5.0007615 224110.
[46] L.-P. Wang, C. Song, Geometry optimization made simple with translation and rotation coordinates, J. Chem. Phys. 144 (2016), https://doi.org/10.1063/1.4952956 214108.
[47] S. Grimme, J. Antony, S. Ehrlich, H. Krieg, A consistent and accurate ab initio parametrization of density functional dispersion correction (DFT-D) for the 94 elements H-Pu, J. Chem. Phys. 132 (2010), https://doi.org/10.1063/1.3382344 154104.
[48] M.A. Salem, K.P. Katin, S. Kaya, A.I. Kochaev, M.M. Maslov, Interaction of dopants and functional groups adsorbed on the carbon fullerenes: Computational study, Physica E 124 (2020) 114319, https://doi.org/10.1016/j.physe.2020.114319.
[49] A.R. Oganov, C.W. Glass, Crystal structure prediction using ab initio evolutionary techniques: Principles and applications, J. Chem. Phys. 124 (2006), https://doi.org/10.1063/1.2210932 244704.
[50] J. Lv, Y. Wang, L. Zhu, Y. Ma, Particle-swarm structure prediction on clusters, J. Chem. Phys. 137 (2012), https://doi.org/10.1063/1.4746757 084104.
[51] D.V. Ignat'eva, A.A. Goryunkov, I.N. Ioffe, L.N. Sidorov, Trifluoromethylation of Fullerenes: Kinetic and Thermodynamic Control, J. Phys. Chem. A. 117 (48) (2013) 13009–13017, https://doi.org/10.1021/jp409249y.
[52] İ. Muz, M. Kurban, Enhancement of Electronic, Photophysical and Optical Properties of 5,5′-Dibromo-2,2′-Bithiophene Molecule: New Aspect to Molecular Design, Opto-Electron. Rev. 27 (2) (2019) 113, https://doi.org/10.1016/j.opelre.2019.03.002.
[53] İ. Muz, M. Atiş, O. Canko, E.K. Yıldırım, *Ab Initio* Search for Global Minimum Structures of Neutral and Anionic Hydrogenated Li5 Clusters, Chem. Phys. 418 (2013) 14, https://doi.org/10.1016/j.chemphys.2013.04.002.
[54] İ. Muz, O. Canko, M. Atiş, E.K. Yıldırım, Search for the Global Minimum Structures of AlB3H(2n) (n = 0–6) Clusters, J. Comput. Chem. 36 (6) (2015) 385, https://doi.org/10.1002/jcc.23812.
[55] M. Rezaian, R. Maleki, M. Dahri Dahroud, A. Alamdari, M. Alimohammadi, pH-Sensitive Co-Adsorption/Release of Doxorubicin and Paclitaxel by Carbon Nanotube, Fullerene, and Graphene Oxide in Combination with N-isopropylacrylamide: A Molecular Dynamics Study, Biomolecules 8 (2018) 127, https://doi.org/10.3390/biom8040127.
[56] K. Butowska, W. Kozak, M. Zdrowowicz, S. Makurat, M. Rychłowski, A. Hać, A. Herman-Antosiewicz, J. Piosik, J. Rak, Cytotoxicity of doxorubicin conjugated with C60 fullerene. Structural and *in vitro* studies, Struct. Chem. 30 (6) (2019) 2327–2338, https://doi.org/10.1007/s11224-019-01428-4.
[57] R.R. Panchuk, S.V. Prylutska, V.V. Chumak, N.R. Skorokhyd, L.V. Lehka, M.P. Evstigneev, Y.I. Prylutskyy, W. Berger, P. Heffeter, P. Scharff, U. Ritter, R.S. Stoika, Application of C_{60} Fullerene-Doxorubicin Complex for Tumor Cell Treatment *In Vitro* and *In Vivo*, J. Biomed. Nanotechnol. 11 (2015) 1139–1152, https://doi.org/10.1166/jbn.2015.2058.
[58] H. Prinzbach, A. Weiler, P. Landenberger, F. Wahl, J. Wörth, L.T. Scott, M. Gelmont, D. Olevano, B.V. Issendorff, Gas-phase production and photoelectron spectroscopy of the smallest fullerene, C20, Nature. 407 (2000) 60–63, https://doi.org/10.1038/35024037.
[59] K.P. Katin, A.I. Podlivaev, Dynamic characteristics of the low-temperature decomposition of the C_{20} fullerene, Phys. Solid State. 52 (2) (2010) 436–438.
[60] F. Wahl, A. Weiler, P. Landenberger, E. Sackers, T. Voss, A. Haas, M. Lieb, D. Hunkler, J. Wörth, L. Knothe, H. Prinzbach, Towards Perfunctionalized Dodecahedranes—En Route to C_{20} Fullerene, Chem. Eur. J. 12 (24) (2006) 6255–6267, https://doi.org/10.1002/chem.200501618.
[61] J. Jia, H.-S. Wu, X.-H. Xu, X.-M. Zhang, H. Jiao, Fused Five-Membered Rings Determine the Stability of C60F60, J. Am. Chem. Soc. 130 (12) (2008) 3985–3988, https://doi.org/10.1021/ja078159010.1021/ja0781590.s002.
[62] W. Zhang, M. Dubois, K. Guérin, P. Bonnet, H. Kharbache, F. Masin, A.P. Kharitonov, A. Hamwi, Effect of curvature on C-F bonding in fluorinated carbons: from fullerene and derivatives to graphite, Phys. Chem. Chem. Phys. 12 (6) (2010) 1388–1398.
[63] V. Schettino, M. Pagliai, L. Ciabini, G. Cardini, The Vibrational Spectrum of Fullerene C60, J. Phys. Chem. A. 105 (50) (2001) 11192–11196, https://doi.org/10.1021/jp012874t.
[64] E. Alimohammadi, R. Maleki, H. Akbarialiabad, M. Dahri, Novel pH-responsive nanohybrid for simultaneous delivery of doxorubicin and paclitaxel: an in-silico insight, BMC Chem. 15 (2021), https://doi.org/10.1186/s13065-021-00735-4.
[65] S. Karimzadeh, B. Safaei, T.-C. Jen, Theoretical investigation of adsorption mechanism of doxorubicin anticancer drug on the pristine and functionalized single-walled carbon nanotube surface as a drug delivery vehicle: A DFT study, J. Mol. Liq. 322 (2021), https://doi.org/10.1016/j.molliq.2020.114890 114890.
[66] H. Wang, A Density Functional Investigation of Fluorinated B12N12 Clusters, Chin. J. Chem. 28 (10) (2010) 1897–1901, https://doi.org/10.1002/cjoc.201090316.
[67] S. Berski, Z. Latajka, A.J. Gordon, On the multiple B-N bonding in boron compounds using the topological analysis of electron localization function (ELF), New J. Chem. 35 (1) (2011) 89–96.
[68] Md Rakib Hossain, Md Mehade Hasan, S. Ud Daula Shamim, T. Ferdous, Md Abul Hossain, F. Ahmed, First-principles study of the adsorption of chlormethine anticancer drug on C24, B12N12 and B12C6N6 nanocages, Computational Theor. Chem. 1197 (2021), https://doi.org/10.1016/j.comptc.2021.113156.
[69] A.S. Rad, K. Ayub, A comparative density functional theory study of guanine chemisorption on $Al_{12}N_{12}$, $Al_{12}P_{12}$, $B_{12}N_{12}$, and $B_{12}P_{12}$ nano-cages, J. Alloy. Compd. 672 (2016) 161–169, https://doi.org/10.1016/j.jallcom.2016.02.139.